Accepted Manuscript

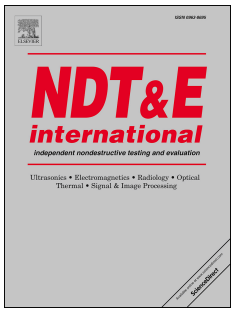

Experimental studies of the magneto-mechanical memory (MMM) technique using permanently installed magnetic sensor arrays

Zhichao Li, Steve Dixon, Peter Cawley, Rollo Jarvis, Peter B. Nagy, Sandra Cabeza

PII: S0963-8695(17)30012-9

DOI: 10.1016/j.ndteint.2017.07.019

Reference: JNDT 1905

To appear in: *NDT and E International*

Received Date: 6 January 2017

Revised Date: 20 June 2017

Accepted Date: 20 July 2017

Please cite this article as: Li Z, Dixon S, Cawley P, Jarvis R, Nagy PB, Cabeza S, Experimental studies of the magneto-mechanical memory (MMM) technique using permanently installed magnetic sensor arrays, *NDT and E International* (2017), doi: 10.1016/j.ndteint.2017.07.019.

Experimental Studies of the Magneto-Mechanical Memory (MMM) Technique Using Permanently Installed Magnetic Sensor Arrays

Zhichao Li[a,*], Steve Dixon[a], Peter Cawley[b], Rollo Jarvis[b], Peter B. Nagy[b,c] and Sandra Cabeza[d]

[a] *Department of Physics, University of Warwick, Coventry, CV4 7AL, UK*

[b] *Department of Mechanical Engineering, Imperial College London, London, SW7 2AZ, UK*

[c] *Department of Aerospace Engineering & Engineering Mechanics, University of Cincinnati, Cincinnati, OH 45221, USA*

[d] *Federal Institute of Materials Research and Testing- BAM, Unten den Eichen 87, Berlin, 12205, Germany*

*Corresponding author: zhichao.li@warwick.ac.uk

Abstract: The magneto-mechanical memory (MMM) method, that is often referred to as the metal magnetic memory method, has been reported to be a non-destructive testing technique capable of quantifying stress concentrations and detecting defects in ferromagnetic materials. The underlying mechanism behind MMM has been explained in the literature, but the sensitivity to stress concentration has not been satisfactorily investigated. In this paper, both the normal and tangential components of the stress-induced MMM signal were measured by permanently installed magnetic sensor arrays on specimens made from three grades of L80 alloy steel and 20 other structural steels; tests were also carried out on a pipe made from the 4140-L80 steel. As expected, the stress history affects the MMM signal, but the experimental results show that significant irreversible change of magnetization always occurs only in the first cycle of loading regardless whether the deformation is purely elastic or partially plastic. If the peak stress level is increased at a given point during cycling, the immediately following

next cycle acts as a new “first” cycle at that peak stress level and causes additional significant irreversible change of magnetization, but there is no evidence that plastic deformation might build up a cumulative magnetization. The MMM effect is very small in the steel samples tested, indicating that it will not be useful in field applications. In un-notched specimens the irreversible change in magnetization caused a proportional change in the measured external magnetic field on the order of only 5-10 A/m, while in the case of notched specimens the leakage field was on the order of 30-60 A/m.

Keywords: magneto-mechanical memory, stress concentration, permanently installed sensors, irreversible change, cumulative magnetization

1. Introduction

Internal or external corrosion in pipelines is unavoidable, and compromises the structural integrity of the pipeline [1]. The pressure and bending stresses that the pipe experiences will result in stress concentrations in corroded areas due to geometric wall thinning. The ability to detect and quantify a stress concentration zone (SCZ) or detect micro-defect growth, can in principle enable one to predict the location of mechanical failure and evaluate the residual life of pipelines [2]. There is a range of well-established non-destructive testing (NDT) methods used in pipeline inspection, such as radiography, ultrasonic testing, eddy current testing and magnetic flux leakage (MFL) pipeline pigs [3]. The magneto-mechanical memory (MMM) technique, which is also referred to as the metal magnetic memory technique [4-7], is promoted as a passive, non-contact NDT method, that uses measurement of the residual magnetic leakage field (RMLF) above a pipe to detect regions of stress concentration or defects [5,8-12].

Ferromagnetic materials exhibit intrinsic remanent magnetization left behind after the applied magnetic field is removed. This magnetic memory effect is widely exploited in

magnetic storage devices and can be also exploited for the purposes of nondestructive materials characterization. Of particular interest in this study was magnetic memory of the mechanical deformation history of ferromagnetic materials that can be directly related to remaining strength and service life of fracture critical components. The underlying physical phenomenon behind such magnetic memory of a mechanical origin is the so-called magneto-mechanical effect [6,13,14], in which the application of stress in a ferromagnetic material causes the rearrangement of magnetic domains, thereby causing a change in the magnetization of the material. The MMM method is generally rather weak and perceivable only in the absence of strong applied magnetic fields. Therefore these NDE techniques require high detection sensitivities commonly encountered in residual magnetic flux leakage measurements. Jiles and Atherton laid down the foundation of NDE based on the elastic magneto-mechanical effect [13,14], which shows that the largest change in RMLF is always in the very first elastic loading cycle. Then, further cycling at the same stress level has no significant effect on the RMLF signal. Dubov reported stronger cumulative elastic and plastic magneto-mechanical effects that he called the "magnetoelastic" effect [5] and "magnetoplastics" [6], respectively. These effects were reported to manifest themselves in an irreversible increase of RMLF in the presence of a weak external field, as shown in Fig. 1. Dubov postulated that cyclic plastic strain has a cumulative effect, so that the RMLF increases right up to point of failure. This effect would make defects producing stress concentrations in heavily loaded structures progressively easier to detect as failure approaches, and could be a very attractive approach for NDT. However, before basing an inspection procedure on the method, it is necessary to determine the strength of the effect in the materials of interest. The magneto-mechanical effect is sensitive to the microstructure of the ferromagnetic material, meaning that mechanical cyclic softening or strengthening can be observed on different materials [15].

A potentially significant advantage of the MMM technique as a means to locate stress concentration or monitor defects is that the signal intensity is not as significantly affected by the stand-off as other techniques such as ultrasound or eddy current inspection [3,16]. This could allow the technique to be applied for detection of corrosion under insulation or in buried pipes at significant stand-off [17]. The MMM technique has been implemented as a periodic screening inspection tool by measuring RMLF distribution on the outer surface of a specimen [18]. It has been reported to be capable of evaluating the degree of stress concentration [19-22], indicating the deformation stage [23-26], and monitoring fatigue crack propagation [27-29].

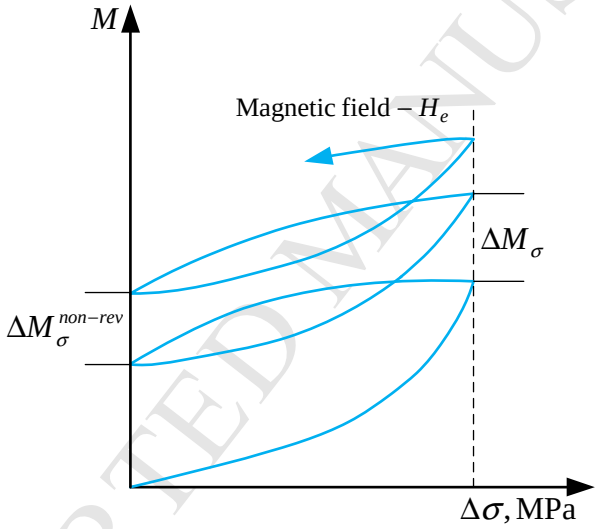

FIGURE 1. Schematic representation of the magnetoelastic effect action mechanism (after [6]): ΔM_σ and $\Delta M_\sigma^{non-rev}$ are variations of residual magnetization under load and after its relief, respectively, $\Delta\sigma$ is the variation of thermal stress and H_e is the external magnetic field.

Recent publications have suggested that the MMM technique has low reliability when used for stress assessment if the formation conditions of the remanence state are not taken into account [30-32]. Different formation conditions may cause significant variation in remanent magnetization. The RMLF produced due to stress concentration depends on many factors, such as the initial magnetic state [33], the external background magnetic field [34,35], the chemical composition and microstructure of the material [15,35] and the load

history [36]. In most MMM experiments in the published literature, the chemical composition of samples was known in advance, and the samples were usually demagnetized prior to the application of stress. As the source of excitation in the MMM technique, the background magnetic field only changes the MMM signal magnitude, and does not change the profile of the response curves. The load history has a more complex influence on the MMM signal, due to the hysteresis of the magneto-mechanical effect [13,36].

During site trials, the MMM technique has been shown to detect defects in some instances, but has failed in other trials [37]. It is interesting to note that diagrams of the form of Fig. 1 are often presented in a schematic form in papers on the MMM technique [5,6,38], rather than being illustrated with real experimental data. In this paper we evaluate the sensitivity of the MMM technique using permanently installed monitoring systems on some steel alloys commonly used in pipeline applications. The primary question this study raises is whether the magnetic memory exhibited by some common Grades of L80 pipe steel conforms to the relatively weak magneto-mechanical effect predicted by Jiles and Atherton [13,14] or to the empirical observations of a stronger cumulative magnetoplastic effect reported by Dubov [6] and others. Both effects occur in the presence of weak external magnetic fields such as the natural geomagnetic field (30-50 A/m).

In this paper, dog-bone specimens were prepared from representative materials and tensile testing was carried out. In addition, four point bending tests were performed on a pipe specimen. Both the normal and tangential components of the stress-induced RMLF just above the specimen surface were measured by means of permanently installed magnetic sensor arrays. Two types of notches were machined in the dog-bone specimens to introduce local stress concentration. The variations of the MMM signal during elastic and plastic deformation during the loading process under different strength biasing magnetic fields were investigated. Tests were also carried out on a pipe made from one of the materials in four

point bending in order to investigate whether similar effects were seen in geometries more representative of industrial practice.

2. Experimental set-ups and samples

2.1. Specimen preparation

Samples were prepared from three different grades of L80 alloy steel [39], which are commonly used for pipelines in the petrochemical industry, and from 20 other structural steels [40-45]. The chemical composition and mechanical properties of these steels are shown in Table I and Table II in the Appendix, respectively. The 5 mm thick, flat, dog-bone shape specimens were machined from pipes of various diameters and wall thicknesses or plates of various lengths and widths, with the dimensions shown in Fig. 2.

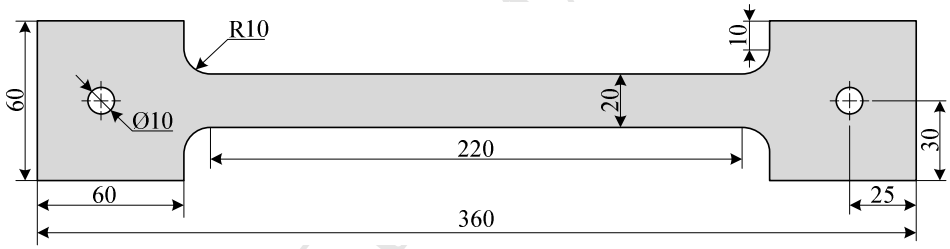

FIGURE 2. Geometry and dimensions of the dogbone specimen (units: mm).

One 450 mm long pipe specimen was prepared for a four point bending test. The material of the pipe specimen was 4140-L80 with outer diameter 60.32 mm and wall thickness 4.83 mm.

2.2. Experimental instrumentation

An Instron 1185 testing machine, whose load error is ±0.5%, was used to carry out the tensile tests on the dog-bone specimens and a Testometric 100 kN FS machine was used to carry out the four point bending test on the pipe specimen. To reduce the influence of surrounding ferromagnetic materials, the specimen clamps for the tensile test and the loading cells for the bending test were made of non-magnetic stainless steel.

The normal and tangential components of the stress-induced RMLF, which are known as the MMM signal, were measured by two permanently installed magnetic sensor arrays. Each magnetic sensor array consists of 16 channels (8 normal channels and 8 tangential channels) of AMR sensors AFF755B, whose resolution is 0.0016 A/m and sensitivity is 15 (mV/V)/(kA/m) [46].

For the dog-bone samples, two linear AMR sensor arrays were fixed on the sides of the specimen surface to isolate magnetic fields originating inside the specimen. The 16 channels of AMR sensors were labeled 1 to 16 and fixed on two 3D printed ABS plastic sensor holders, as shown in Fig. 3. The tangential magnetic field sensors were marked by odd numbers (blue colour), while the normal ones were marked by even numbers (orange colour). Here, the “normal magnetic field” component is in the direction normal to the specimen surface, while the “tangential magnetic field” is in the direction parallel to the specimen surface in the length direction of the sample. The tangential and normal magnetic field sensors were placed alternately in the length direction. The designations f and b represent the front face and back face, respectively.

Two ring AMR sensor arrays were fixed on the outer surface of the pipe specimen, as shown in Fig. 4. The tangential magnetic field sensors were marked by odd numbers (blue colour), while the normal ones were marked by even numbers (orange colour). Here, the “normal magnetic field” component is in the direction normal to the pipe surface, while the “tangential magnetic field” is in the direction parallel to the specimen surface in the axial direction of the pipe. The tangential and normal magnetic field sensors were placed alternately in the circumferential direction.

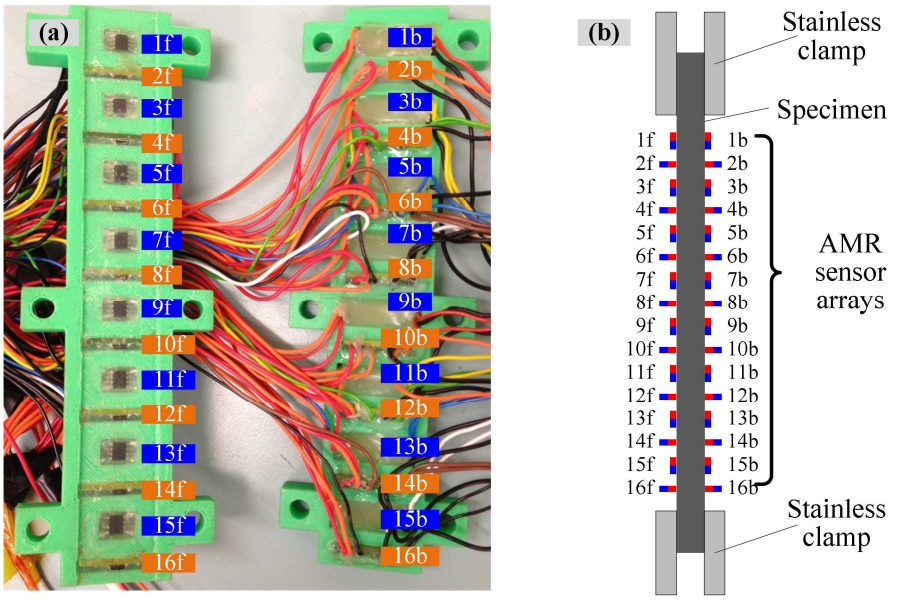

FIGURE 3. (a) Photograph and (b) schematic diagram of the configuration of two AMR sensor arrays. The tangential magnetic field sensors were marked by odd numbers (blue colour), while the normal ones were marked by even numbers (orange colour) in (a). The designations f and b represent the front face and back face of the sample, respectively.

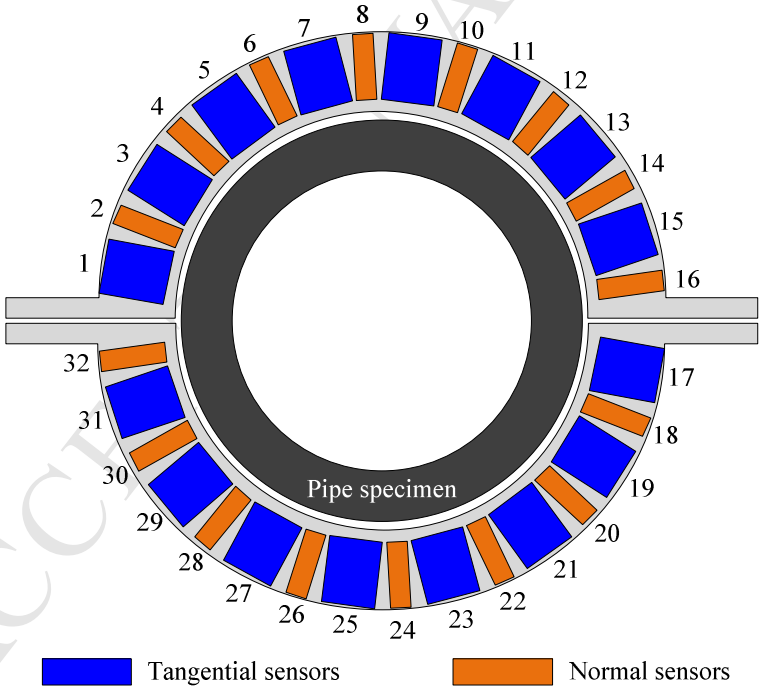

FIGURE 4. Schematic diagram of the configuration of the ring AMR sensor arrays. The tangential magnetic field sensors were marked by odd numbers (blue colour), while the normal ones were marked by even numbers (orange colour).

An electrical circuit was designed to control the 32 channels of AMR sensors, as shown in Fig. 5. In Fig. 5, the shape of the AMR sensor arrays can be either linear or ring and the

corresponding specimen is either a dog-bone sample or pipe sample. The AMR sensors were powered by a constant voltage power supply. The multiplexer, which consists of 4×16 channels, was divided into two groups and controlled by a Pico data logger to switch the differential outputs of the AMR sensors into a two channel amplification circuit. The amplified voltages were captured by the Pico data logger and then sent to a PC for post processing.

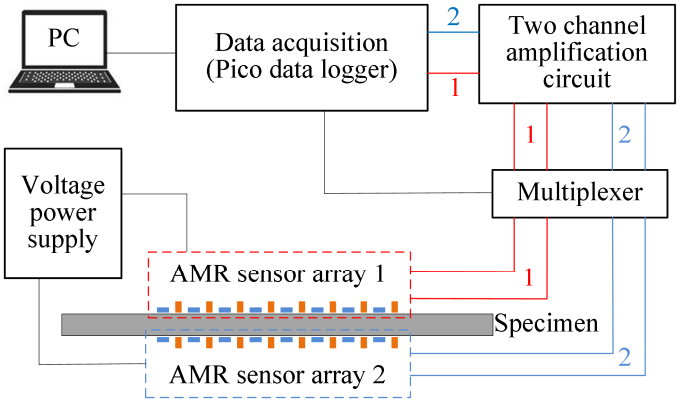

FIGURE 5. Schematic diagram of hardware circuit.

3. Experimental procedure

Five experiments were conducted in this study. Firstly, one 4140-L80 dog-bone specimen was chosen to study the elastic magneto-mechanical effect described by Jiles and Atherton [13,14]. Secondly the strength of the plastic magneto-mechanical effect on three kinds of L80 dog-bone specimens was checked under plastic deformation. Next, two types of notches were machined on 4140-L80 dog-bone specimens in order to investigate whether the effects were stronger in the presence of localized change of the sort that would be of interest to detect. Some pipelines are routinely inspected by 'pigging' using the magnetic flux leakage (MFL) technique and this leaves significant remnant magnetisation [47]. It was therefore also of interest to investigate whether the presence of remnant magnetization affected the MMM measurements.

It should also be remembered that the geometry of the dog-bone sample used should produce a stronger MMM signal than would be observed in a pipe specimen for the same level of applied stress. This is because one would expect the magnetic return path in a pipe geometry to reduce the amount of magnetic flux leakage when compared to the dog-bone sample shape. Therefore, a four point bending test was carried out on a pipe specimen to study the elastic magneto-mechanical effect.

These experiments were carried out at room temperature and in the presence of the Earth's magnetic field (horizontally northward 15.12 A/m and vertical component perpendicular down to the Earth's surface 35.81 A/m). Before testing, all the specimens were demagnetized by a Magnaflux L-10 coil to eliminate any magnetization generated during machining.

3.1. Magnetization change under elastic load

To study the elastic magneto-mechanical effect, a 4140-L80 dog-bone specimen was loaded to 250 MPa (about 45% of the yield strength). Instead of loading the specimen direct to 250 MPa, the load was increased in three steps:

(1) Two load and unload cycles from 0 to 100 MPa with readings taken at 10 MPa steps, without demagnetizing between cycles.

(2) Two load and unload cycles from 0 to 180 MPa with readings taken at 10 MPa steps, without demagnetizing.

(3) Two load and unload cycles from 0 to 250 MPa with readings taken at 10 MPa steps, without demagnetizing.

By increasing the load in steps, the magnetization change due to first loading cycle and further cycling at the same stress level can be clearly distinguished. Two linear AMR sensor arrays as shown in Fig. 3 were fixed on both sides of the dog-bone specimen using brass screws. The lift-off distance between AMR sensors and the specimen surface was 1 mm.

3.2. Magnetization change under plastic load

Three types of L80 dog-bone specimens were used to study the plastic magneto-mechanical effect based on the mechanical properties given in Table 2:

(1) 4140-L80 cycled up to 20% strain in 5% steps, without demagnetizing.

(2) 9CR-L80 cycled up to 0.5% strain in 0.1% steps, without demagnetizing.

(3) 13CR-L80 cycled up to 0.5% strain in 0.1% steps, without demagnetizing.

The MMM signal was measured by the same linear AMR sensor arrays simultaneously when applying the load. To measure the strain, four strain gauges were used to make a Wheatstone bridge. One strain gauge was attached on the specimen surface and the other three were used as references. A photograph of the AMR sensor array and strain gauge configuration is shown in Fig. 6.

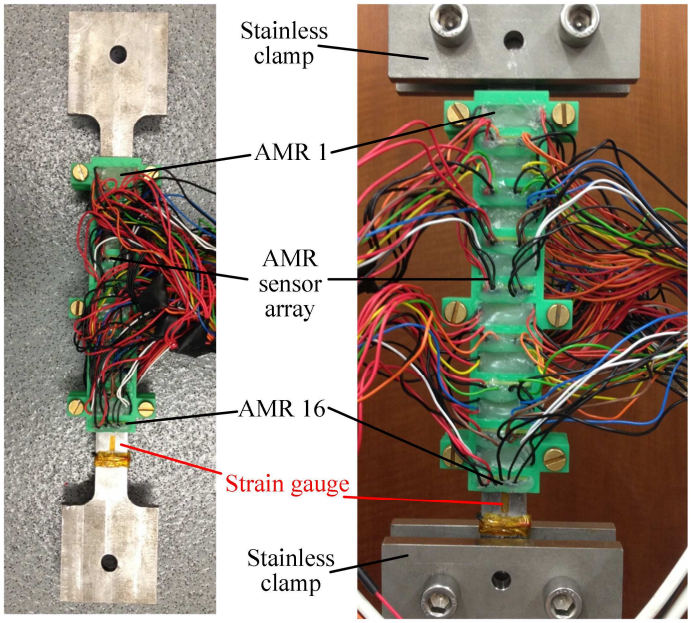

FIGURE 6. Photograph of AMR sensor array and strain gauge configuration for plastic tests.

3.3. Notched samples

In order to produce local stress concentration during loading, two types of notches were machined in the center of two 4140-L80 dog-bone specimens labeled A and B, respectively. Specimen A was machined with two semi-cylindrical notches on the face surfaces, as shown in Fig. 7(a). Specimen B was machined with two semi-cylindrical notches on the side surfaces, as shown in Fig. 7(b). The dimensions of the notches are listed in Table 1.

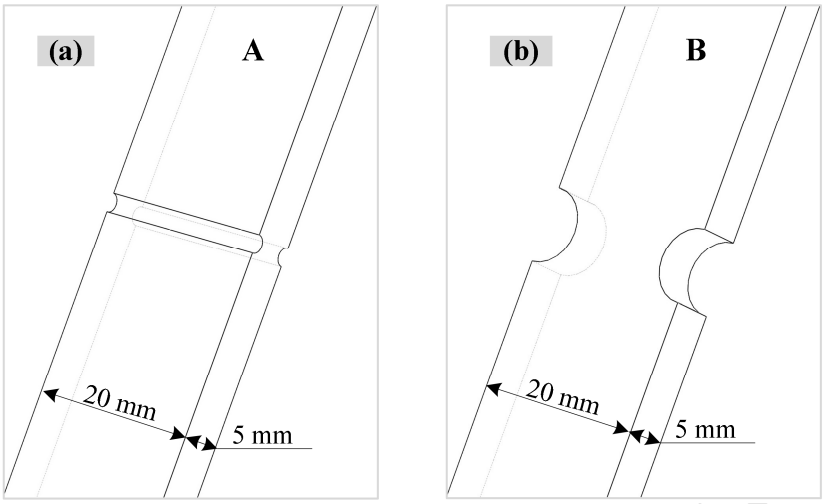

FIGURE 7. Schematic diagram of two types of notches in the center of 4140-L80 dog-bone specimens. (a) Notches on face surfaces of specimen A and (b) notches on side surfaces of specimen B.

TABLE 1. Dimensions of two types of notches.

	Notch type	Notch diameter (mm)	Notch depth (mm)
Specimen A	Face-notched	2	1
Specimen B	Side-notched	8	4

The MMM signal from the notched samples was measured using the same linear AMR sensor arrays as already described, in the following steps:

(1) Demagnetize the dog-bone specimen.

(2) Measure the MMM signal with no load at different levels of biasing magnetic field, which was generated by a Helmholtz coil, as shown in Fig. 8. The Helmholtz coil, with a diameter of 300 mm, was placed horizontally and in the East-West direction.

(3) Demagnetize the specimen.

(4) Increase the load in 50 MPa steps to a nominal average stress of approximately 600 MPa and then unload in 50 MPa steps. Take magnetic measurements at each load step.

(5) Demagnetize the specimens.

(6) Repeat the measurement of the MMM signal with no load at different levels of biasing magnetic field.

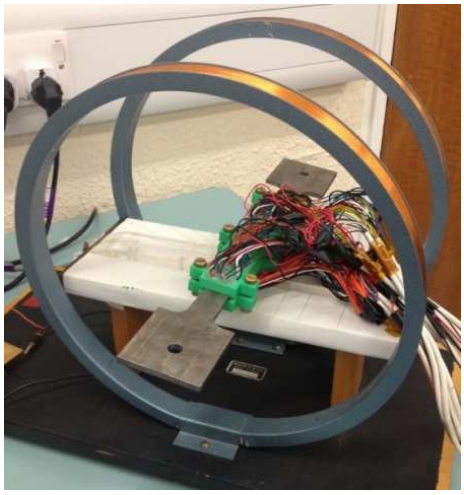

FIGURE 8. Helmholtz coil generates different levels of magnetization.

3.4. Side notched sample with remanent magnetization

The same side notches as shown in Fig. 7 (b) were machined on a new 4140-L80 dog-bone sample labeled as "C". To study the influence of remanent magnetization on the MMM signal, the sample was demagnetized and then put into a magnetizing solenoid coil to obtain a remanent magnetization of approximately 300 A/m in the sample. The solenoid coil, which has a diameter and length of 65 mm and 330 mm respectively, is constructed from 1000 turns of 28 gauge, insulated copper wire. The DC resistance of the solenoid coil was 157 Ω +/-5%. After magnetization, the dog-bone sample was loaded in 50 MPa steps to a nominal average stress of approximately 600 MPa and then unloaded in 50 MPa steps. Magnetic measurements were taken at each load step.

3.5. Magnetization change of pipe sample under a four point bending test

A four point bending test was performed on a pipe specimen to study the stress-induced RMLF in the magnetic return path of a pipe geometry. A schematic diagram of the four point bending test is shown in Fig. 9. The span distances of L_1, L_2 and L_3 are the same (L_1= L_2= L_3=100 mm). To reduce stress concentration at the loading points, four aluminum sheets (4 mm thick) were inserted into the contacting area between the rollers and the pipe sample. One pair of strain gauges (pair I) were placed in the center part of the pipe sample, with one on the

top and the other one on the bottom; another pair of strain gauges (pair II) were placed near the left supporting roller.

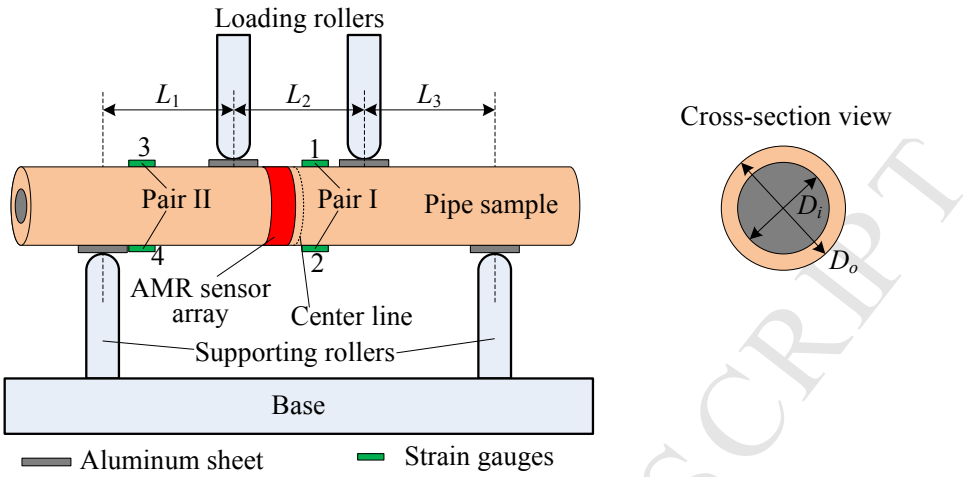

FIGURE 9. Schematic diagram of the four point bending test. L_1= L_2= L_3=100 mm, and the maximum force loaded at each roller is 50 kN.

The flexural stress in the four point bending test can be estimated from simple beam theory [48], the maximum stress when a 50 kN load was applied at each loading roller being 462 MPa. Instead of loading the specimen direct to this maximum stress, the load was increased in three steps:

(1) Two load and unload cycles from 0 to 154 MPa with readings taken at 10 MPa steps, without demagnetizing between cycles.

(2) Two load and unload cycles from 0 to 308 MPa with readings taken at 10 MPa steps, without demagnetizing between cycles.

(3) Two load and unload cycles from 0 to 462 MPa with readings taken at 10 MPa steps, without demagnetizing between cycles.

By increasing the load in steps, the magnetization change due to the first loading cycle and further cycling at the same stress level can be clearly distinguished. Two ring AMR sensor arrays as shown in Fig. 4 were fixed on the outer surface of the pipe specimen using brass screws. The lift-off distance between the AMR sensors and the pipe surface was 1 mm.

3.6. Tests on wider variety of steels with side notches

Having completed the extensive tests above on 4140-L80 steel, a representative test was then carried out on a further 20 steels in order to see whether the same trends were seen. The same side notches as shown in Fig. 7(b) were machined in dog-bone specimens made from these steels. The notched samples were tested in the following steps:

(1) Demagnetize;

(2) Increase load in steps (≤5% yield strength) to a nominal average stress of approximately 10% above the yield stress yield strength and take magnetic measurements at each load step;

(3) Unload in steps (≤5% yield strength) and repeat magnetic measurements at each step.

4. Experimental results and analysis

4.1. Magnetization measurement under elastic load

Our goal was to selectively measure the magnetic field produced by sources inside the specimen by suppressing the magnetic field originating from external sources. Based on the experimental results, it was found that the tangential magnetic field signal does not vary significantly in the area tested, and so to summarize the data for each loading test, the tangential field data from each side of the sample is averaged, as shown in Eq. (1).

$$H_{\text{tangential}} = \frac{\sum H_{nf} + \sum H_{nb}}{\text{number of tangential sensors}} \tag{1}$$

The normal field varies approximately linearly along the length direction and is strongest towards the ends of the sample as expected; the normal field data from the 4 outermost sensors is presented, as shown in Eq. (2). The normal field measured by sensors closer to the specimen centre show small variations during the loading process; data from these sensors have lower SNR and are therefore not used in this summary data.

$$H_{\text{normal}} = \frac{(H_{2f} - H_{16f}) + (H_{2b} - H_{16b})}{4} \quad (2)$$

To present the experimental data more clearly, the raw data was compressed according to Eqs. (1) and (2). After this, the magnetization change during six load cycles can be obtained. It was found that the results on repeat loading cycles to the same maximum load were almost identical to those of the first cycle. The solid and dashed lines indicate the loading and unloading steps, respectively. An irreversible change is seen in initial loading to a given load, while subsequent unloading and reloading gives reversible changes. This finding on the elastic magneto-mechanical effect is completely consistent with that obtained by Jiles and Atherton [13,14], but the effect is small (about 10 A/m maximum compared with the Earth's magnetic field ~40 A/m).

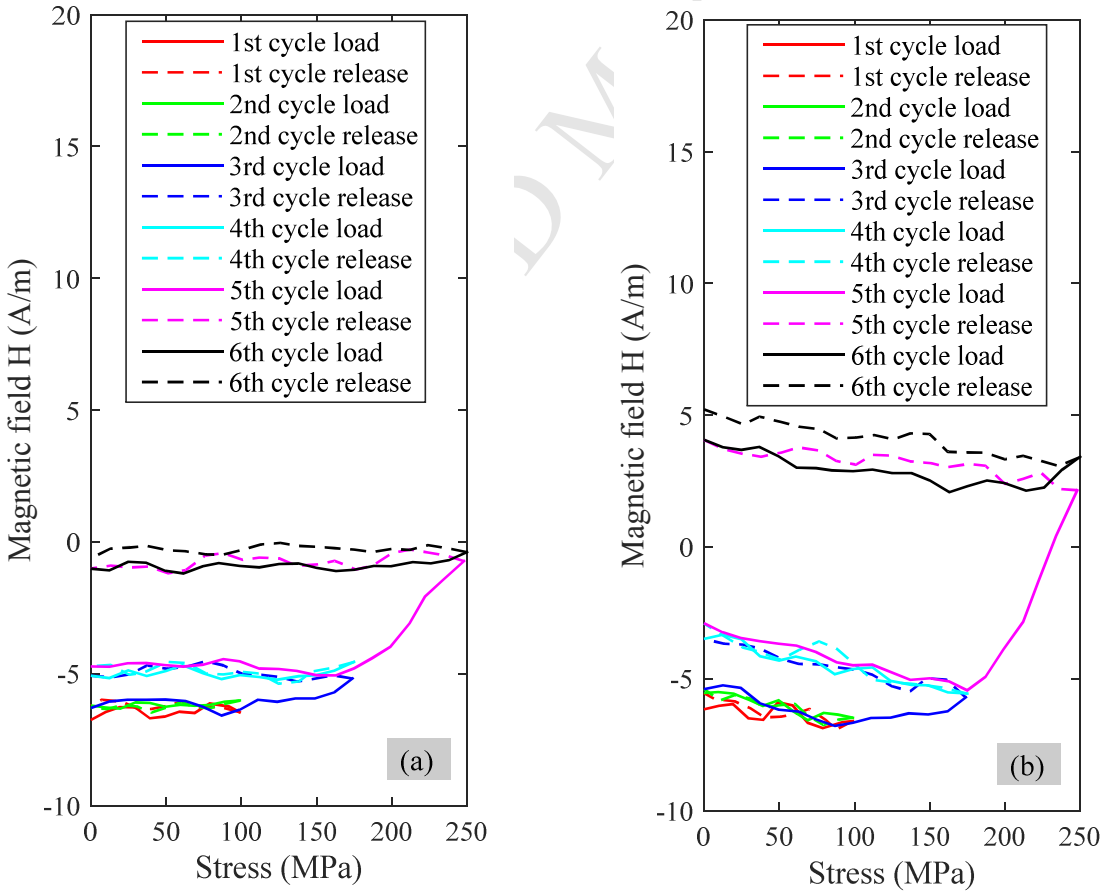

FIGURE 10. (a) Tangential and (b) normal magnetic field change of 4140-L80 dog-bone sample measured during elastic testing. The solid and dashed lines indicate the loading and unloading steps, respectively.

4.2. Magnetization measurement under plastic load

The raw data of magnetization change during plastic tests was compressed according to Eqs. (1) and (2). The curves from repeat measurements at the same strain level were averaged due to the small signal levels. The magnetization change for the 4140-L80 sample during plastic deformation is shown in Fig. 11.

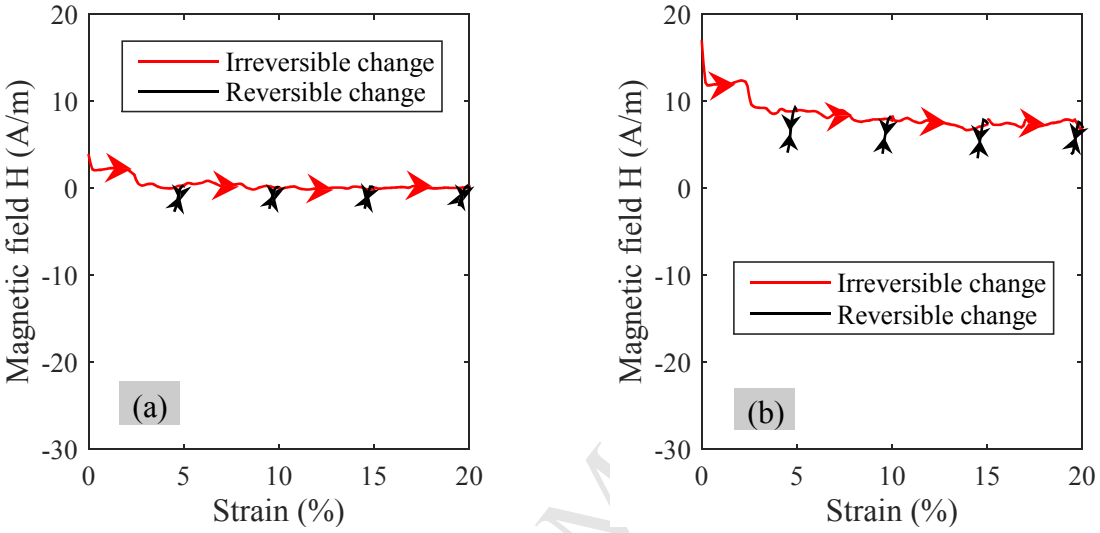

FIGURE 11. (a) Tangential and (b) normal magnetic field change of 4140-L80 sample measured during plastic deformation.

It can be seen that the profile of the tangential magnetic field is similar to that of the normal magnetic field. Likewise, the tangential and normal magnetic fields have similar profiles for the 9CR-L80 and 13CR-L80 samples, except that the signal amplitude is different. Due to the limited space available on the sample surface with the AMR sensors used, only the normal magnetic field was measured for the other two samples, and is shown in Fig. 12. From Fig. 11 and Fig. 12, it can be seen that the stress history affects the MMM signal, but the effects are small in these materials (about 10-20 A/m compared with the Earth's magnetic field of ~40 A/m in the lab), and the plastic deformation tends to reduce the MMM signal. The results show no evidence of the cumulative effect due to cyclic plastic strain reported by Dubov [6]. In this experiment, the plastic strain is essentially uniform along the sample length

direction. Therefore it was decided that localized strain deformation would be introduced in the next stage of the experiments to further check the plastic magneto-mechanical effect.

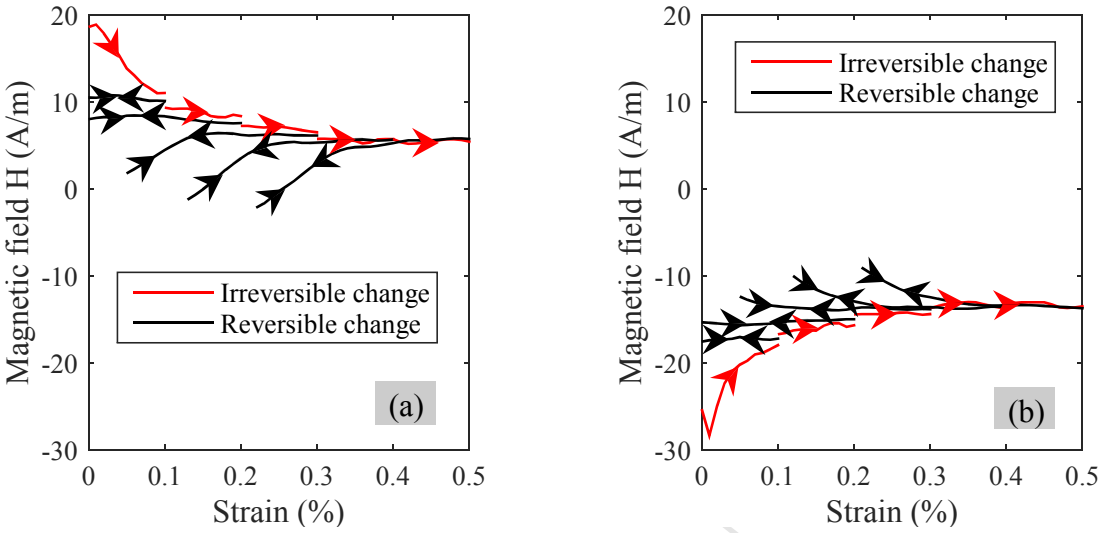

FIGURE 12. Normal magnetic field change of (a) 9CR-L80 and (b) 13CR-L80 samples measured during plastic deformations.

4.3. Magnetization measurement of notched samples

By localizing the plastic strain the localized magnetization becomes easier to detect through the resulting RMLF. Figure 13 presents the experimental results of the face notched sample at different biasing magnetic field before being loaded. The variation of the normal magnetic field at different axial positions is much more obvious than that observed for the tangential magnetic field. Therefore, only the normal field is presented in further results.

The magnetic signal of interest in Fig. 13 is surrounded by incoherent noise which makes analysis of the correlation with the controlled input parameters difficult. A matched filter was therefore proposed which takes advantage of the a-priori knowledge of the system, in order to suppress the noise that does not match the expected behavior of the signal. One must note the limitations of this approach, in that noise that matches the expected behavior of the signal will pass through the filter, and it is only applicable to simple situations with a known specimen geometry and loading process. The filter steps are outlined below:

(1) The general slope of the data was removed as this is only related to the specimen geometry.

(2) The average value of the field was subtracted, as the normal magnetic field on the specimen surface should have odd symmetry with a vanishing average.

(3) The normal magnetic field data equidistant from the sample center were averaged with an inverted sign as the normal field produced by magnetization exhibits odd symmetry about the specimen center (due to the alternation of adjacent normal and tangentially oriented sensors, there was an offset equal to the array pitch between sensors above and below the sample center).

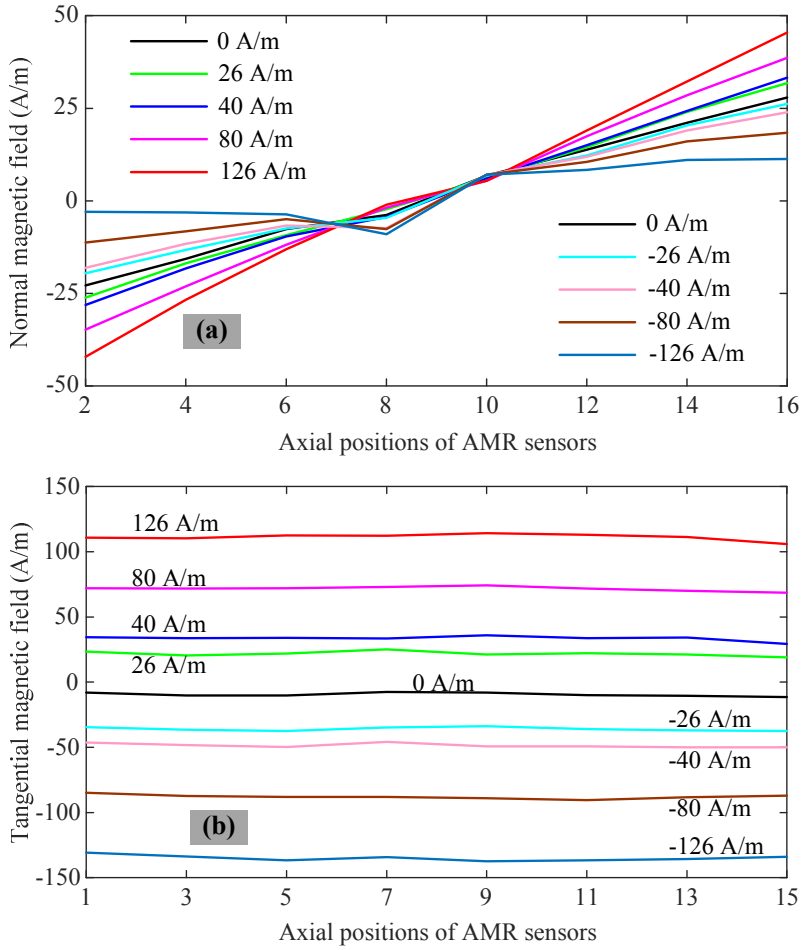

FIGURE 13. Magnetic field measurement of face notched sample at different magnetization levels. (a) Normal magnetic field and (b) tangential magnetic field.

The peak to peak amplitude of the filtered magnetic field was then calculated on sensors 6-12, as these sensors were closest to the notch as shown in Fig. 3. After data processing, comparison of the peak to peak value of the normal magnetic field perturbation under different biasing magnetic fields can be obtained for both types of notched specimens, as shown in Fig. 14. The average value was subtracted as the expected normal magnetic leakage field caused by magnetization inside the specimen is zero. The cross markers are the measured data points and the solid line is the fitted line based on linear regression. As expected, the perturbation generated by the notch is proportional to the applied field, but it is much smaller in magnitude than the applied field. The test was repeated after the samples had been loaded to a nominal average stress of 600 MPa, and it was observed that the effect was increased but was still relatively small.

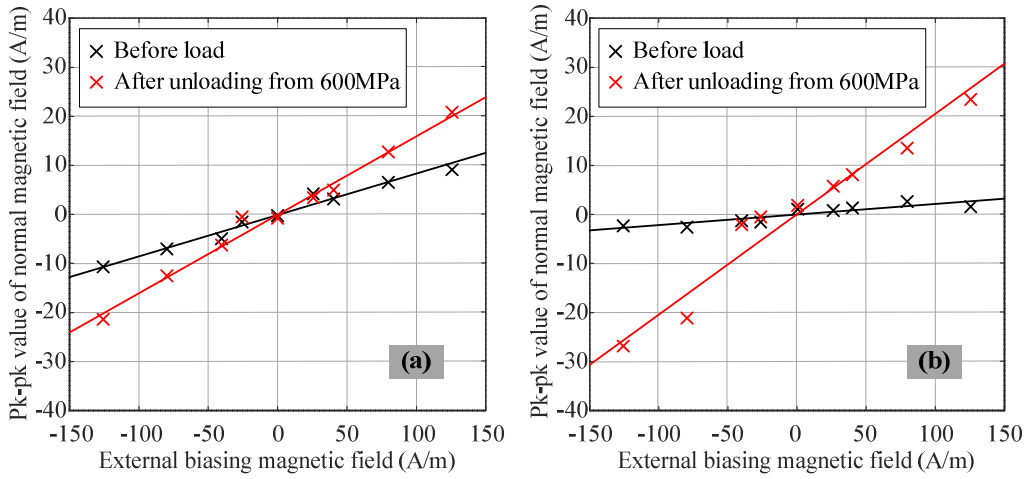

FIGURE 14. Comparison of peak to peak amplitude of the normal magnetic field perturbation from notches as a function of external bias field for (a) the face notched specimen and (b) the side notched specimen.

Figure 14(a) shows that the slope of the fitted curves increases from 8.5% (before load) to 16.1% (after unloading from 600 MPa) for the face notched specimen, while for the side notched specimen the slope increases from 2.3% (before load) to 20.6% (after unloading from 600 MPa), as shown in Fig. 14(b). It can be seen that the plastic deformation and residual stress around the notches after loading will increase the remanent flux leakage. The effect of side notches is larger than that observed for face notches. This is because the side

notches have a larger magnetization concentration length (8 mm) in the length direction of the sample, compared with that of face notches (2 mm), and the spatial resolution of normal magnetic sensors is 20 mm. Therefore the current AMR sensor arrays can capture larger RMLF signal for side notched samples than face notched samples.

The notched dog-bone specimens were also loaded and unloaded in 50 MPa steps. Figure 15 shows the normal magnetic field of the face notched specimen at different loading and unloading steps, where the solid and dashed lines indicate the loading and unloading steps, respectively.

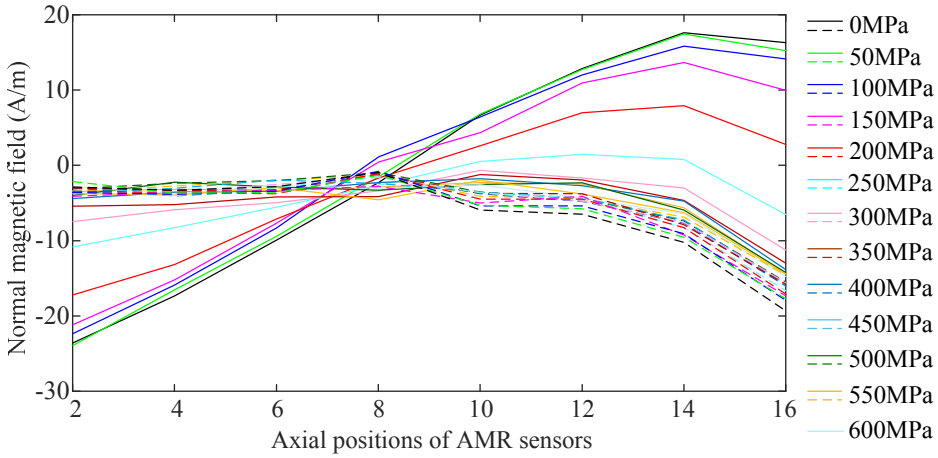

FIGURE 15. Normal magnetic field measured at different loading and unloading steps of face notched sample. The solid and dashed lines indicate the loading and unloading steps, respectively.

The normal component of magnetic field was used for data post-processing by using the filter steps 1-3 outlined previously. Here, the data from the original zero load case was subtracted from all other load cases, so that the remaining magnetic field profiles are only due to stress-induced magnetization. The comparison of the normal magnetic field profiles of the two types of specimens during the loading and unloading steps is shown in Fig. 16.

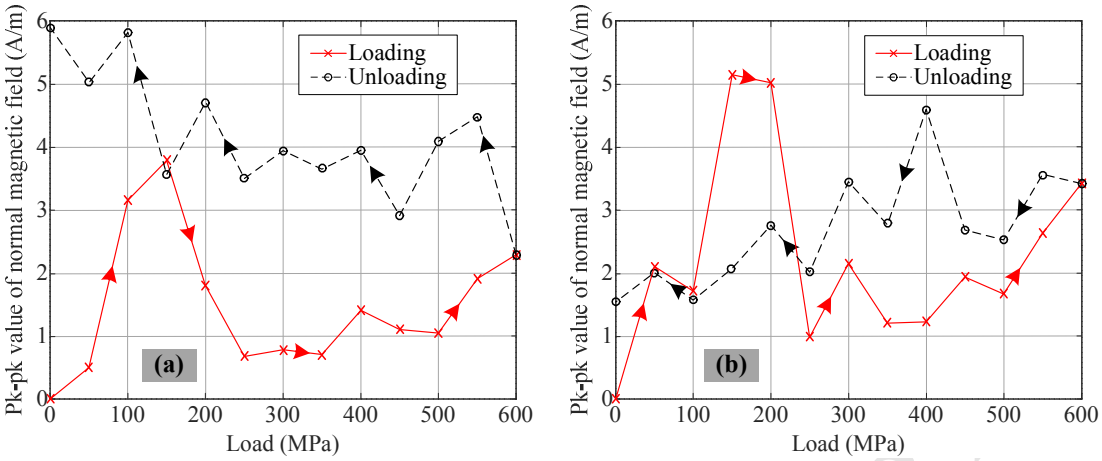

FIGURE 16. Comparison of peak to peak amplitude of the normal magnetic field during loading and unloading steps for (a) face notched specimen and (b) side notched specimen.

When applying the load, plastic deformation and residual stress were generated around the notches. We have confirmed the presence of residual stresses of the order of 200 MPa predicted by finite element (FE) simulations via neutron diffraction measurements [49]. Figure 16 indicates that there is a measurable effect, but again it is very small (about 6 A/m maximum compared with the Earth's magnetic field ~40 A/m) and does not vary monotonically with load. Further tests on different samples have shown that the MMM signals detected are fairly reproducible for each alloy grade tested. The results presented here show no evidence of a cumulative plastic magneto-mechanical effect.

4.4. Magnetization measurement of side notched sample with remanent magnetization

Figure 17 presents the normal magnetic field results of the side notched sample during the loading and unloading process, where the solid and dashed lines indicate the loading and unloading steps, respectively. The dashed lines are overlapped because the magnetization change during unloading process is small.

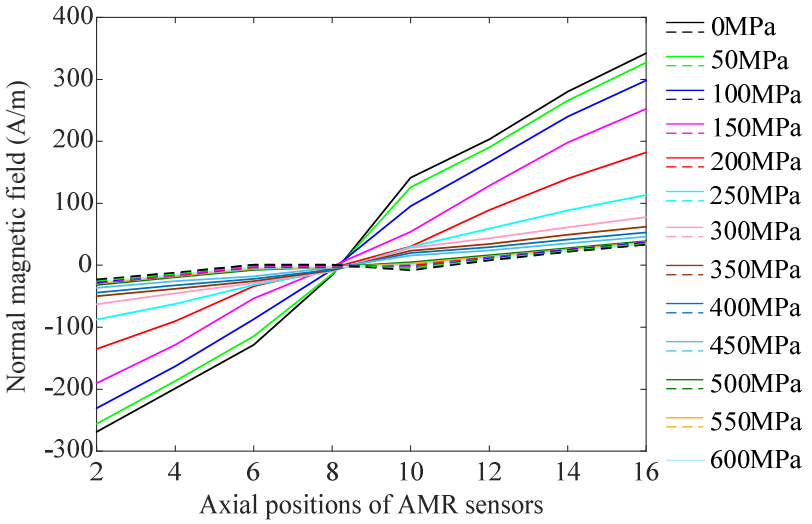

FIGURE 17. Normal magnetic field measured at different loading and unloading steps with remanent magnetization. The solid and dashed lines indicate the loading and unloading steps, respectively.

Based on the matched filter outlined previously, the raw data of the normal magnetic field was processed. The relationship between the magnetization change and loading steps was calculated, as shown in Fig. 18.

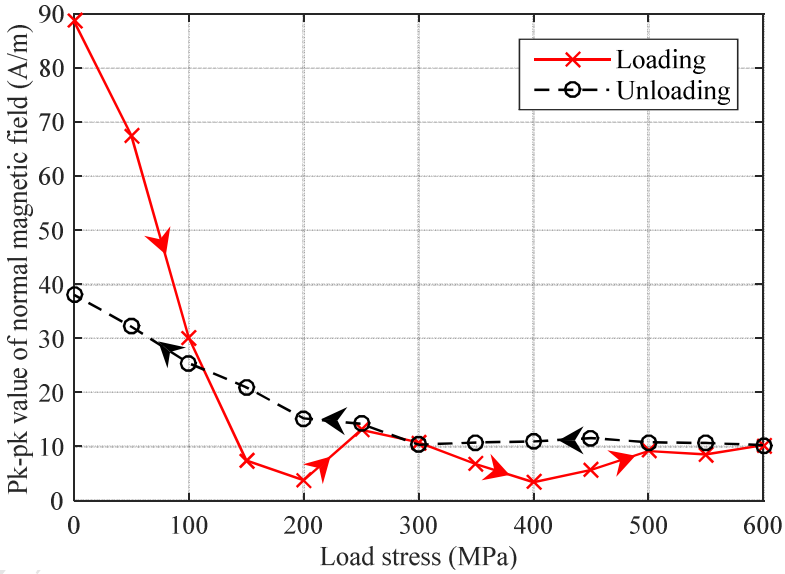

FIGURE 18. Magnetization change during loading and unloading steps for a side notched sample with remanent magnetization.

It can be seen that the remanent magnetization has been significantly decreased with a small applied stress (about 150 MPa). Plastic deformation generated by the notches has a relatively small effect on the MMM signal, as described in the previous section. During the

unloading process, there is a small increase in the normal magnetic field signal with decreasing load. Plastic deformation does not seem to build up a cumulative magnetization; rather, it tends to erase the magnetic memory.

4.5. Magnetization measurement of pipe sample under a four point bending test

Based on the experimental results, it was found that the tangential magnetic field signal does not vary significantly in the area tested. In order to suppress the magnetic field originating from external sources and summarize the data for each loading test, the averaged tangential magnetic field data from the whole circumferential direction of the pipe specimen is presented, as shown in Eq. (3).

$$H_{\text{tangential average}} = \frac{\sum (H_n - H_{n0})\ (n = 1, 3, ..., 31)}{\text{number of tangential sensors}} \tag{3}$$

where H_{n0} is the initial tangential magnetic field.

The normal field almost varies approximately sinusoidally along the circumferential direction of the pipe specimen. To average the normal magnetic field, three steps were used as follows:

(1) The initial normal magnetic field was subtracted as this is related to the remnant magnetization.

(2) The sum values of the top normal sensors ($\sum H_{top}$) and bottom normal sensors ($\sum H_{bottom}$) were calculated, respectively.

(3) The averaged normal field is obtained by

$$H_{\text{normal average}} = \frac{\sum H_{top} - \sum H_{bottom}}{\text{number of normal sensors}} \tag{4}$$

To present the experimental data more clearly, the raw data was compressed according to Eqs. (3) and (4); after this, the magnetization change during six load cycles can be obtained. It was found that the results on repeat loading cycles to the same maximum load were almost

identical to those of the first cycle. Therefore only the average results are presented in Fig. 19, the arrows indicating loading or unloading. An irreversible change is seen in initial loading to a given load, while subsequent unloading and reloading gives reversible changes. However the effect is small (about 25 A/m maximum compared with the Earth's magnetic field ~40 A/m).

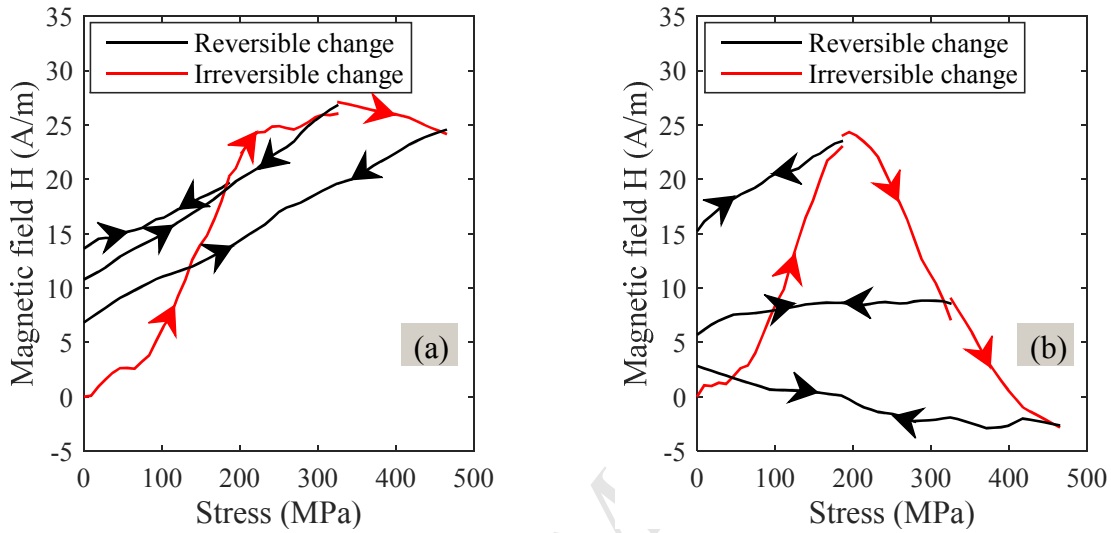

FIGURE 19. (a) Tangential and (b) normal magnetic field change of pipe sample measured during bending test.

The dog-bone sample should produce a stronger MMM signal than the pipe specimen for the same level of applied stress, but Fig. 19 shows that the magnetization change of the pipe specimen is about 25 A/m under 250 MPa stress, while the magnetization change of the dog-bone specimen is 10 A/m under 250 MPa stress as shown in Fig.10. The reason for the larger magnetization change of the pipe specimen is due to the influence of the Testometric machine. There are two support arms of the machine that are made of ferromagnetic material. The gap between the pipe specimen and the arms is small (about 25 mm) so the pipe specimen was in the magnetic return path and the external bias magnetic field was reinforced, which caused a larger magnetization change under the same level of applied stress [13].

The MMM technique has been implemented as a periodic screening inspection tool and reported to be capable of measuring stress concentration and detecting defects. However,

these results indicate that it will not be a useful technique in practice in the field for these steel alloys.

4.6. Variety of steels with side notches

Since complex tests conducted on full-scale pipes produced very similar results to those obtained by much simpler means on simple, small machined specimens, it was decided to investigate whether the cumulative magnetoplastic effect could be found in other materials on the side-notched dog-bone specimen shown in Fig. 7(b) with dimensions listed in Table 1. Specimens of each of 20 structural steels were prepared and loaded and unloaded in steps ($\leqslant$ 5% yield strength). The normal component of magnetic field was processed using the filter steps 1-3 outlined previously in Section 4.3. Figure 16 shows that the peak to peak amplitude of the magnetic field varies with load and this erratic behavior was seen in the tests on all the steels. Table 2 shows the maximum peak to peak amplitude for each steel; from Fig. 16(b), this is 5.2 A/m for the 4140-L80 steel.

TABLE 2. Maximum magnetization change during loading and unloading of different steels.

Steel type	Amplitude of magnetic field (A/m)	Steel type	Amplitude of magnetic field (A/m)
1.0570	5.5	708M40	6.8
1.2083	4.2	EN9	8
1.2312	13	EN32	6.5
1.2343	14	EN42	8
1.2363	9	EN43	5.3
1.2379/D2	7.3	EN45	6.4
1.2436	8.7	EN47	8.4
1.2510/O1	10.1	S275	4.8
1.2767	10	S355J2+N	6
1.7131	6	X65	6.2
4140-L80	5.2	13CR-L80	19.3
9CR-L80	21		

Table 2 indicates that there are measurable MMM effects of the steels tested, but again they are very small (up to about 21 A/m maximum compared with the Earth's magnetic field ~40 A/m). The results presented here also show no evidence of a cumulative plastic magneto-mechanical effect on different steels tested.

5. Discussion

The primary question this study raised was whether the magnetic memory exhibited by common Grade L80 pipe steels and other structural steels conforms to the relatively weak magneto-mechanical effect predicted by Jiles and Atherton [13,14] or to the empirical observations of a stronger cumulative magnetoplastic effect reported by Dubov [6] and others. Both effects occur in the presence of weak external magnetic fields such as the natural geomagnetic field (30-50 A/m). In the case of the well understood ordinary magneto-mechanic effect, application of stress tends to release the pinned domain walls and thereby diminishes the magnetic hysteresis. This leads to an irreversible change of magnetization towards the anhysteretic equilibrium in the material at the prevailing external magnetic field level. This irreversible change towards the anhysteretic equilibrium value could be either positive or negative depending on the initial magnetization. If the material is in a demagnetized initial state, the change of magnetization will be positive, i.e., in the direction of the external magnetic field, because the initial magnetization curve of ferromagnetic materials always lies below the anhysteretic curve [50]. Movement of pinned domain walls is similar to dislocation motion under plastic deformation, but we will reserve the term “plastic” change to irreversible mechanical deformation. Most of the irreversible change of magnetization occurs in the first cycle of loading. However, the anhysteretic magnetization is also slightly stress dependent because of domain-wall bending, a phenomenon analogous to dislocation bending during elastic mechanical deformation, which leads to relatively small reversible changes of magnetization during the following cycles.

Let us consider cycling at the same stress level as earlier shown in Fig. 1. Regardless whether the first cycle is purely elastic or partially plastic, it is the only one that causes relatively large irreversible changes in magnetization. Subsequent fully elastic cycles cause only small reversible changes in magnetization due to the stress-dependence of the

anhysteretic magnetization curve. If the peak stress level is increased at a given point during cycling, the immediately following next cycle will act as a new “first” cycle at that peak stress level and likely cause significant irreversible changes in magnetization. Further cycles up to the previous peak stress level are fully elastic and cause only relatively small reversible changes in magnetization. It is worth citing what Bozorth wrote about this critical issue in his seminal monograph on ferromagnetism [51]: “When H (magnetic field) is applied first and maintained constant, successive applications and release of sigma (stress) cause unequal changes in B (flux density) until the process has been repeated a number of times, thus for the 'cyclic state' the change in B produced by the stress is often considerably less than for the first application of the same stress.”

As described by Dubov [5,6], the so-called Metal Magnetic Memory method is based on a much stronger cumulative process of “self-magnetization” in ferromagnetic bodies. Such self-magnetization occurs when the strain-induced magnetization due to the inverse magnetostrictive effect (also known as Villari effect) is much stronger than the weak external magnetic field. Although there is little doubt that cumulative self-magnetization can occur in ferromagnetic materials when exposed to cyclic deformation in the presence of a weak external magnetic field, very little is known in the scientific literature about the magnitude of this “magnetoplastic” effect in engineering materials such as commonly used pipe steels. There is plenty of evidence that the Metal Magnetic Memory method can be exploited for flaw detection when it is used just like any other residual magnetic flux leakage technique to detect surface-breaking cracks or subsurface ones at shallow depths, though its selectivity is questionable as there are many competing influences on the magnetization of the material [52-54]. However, the use of this NDE method for quantitative materials characterization crucially depends on whether a cumulative process of self-magnetization occurs in typical engineering materials, such as pipe steels, an issue that is highly relevant from the points of

view of both scientific research and engineering applications. The principal experimental results presented in Figs. 10-12, 18, and 19 clearly demonstrate that the behavior of the three common Grade L80 pipe steels (4140-L80, 9CR-L80, 13CR-L80) and twenty other structural steels tested in our study conforms to the weak magneto-mechanical effect predicted by Jiles and Atherton [13,14] and showed no indication of the cumulative magnetoplastic effect that is required for the MMM as described by Dubov et al. to be capable of reliably detecting small area of stress concentration. Distinguishing between these two competing magnetization mechanisms is rendered easy and unequivocal by the fact that in the former case cyclic loading erases rather than builds up the magnetic memory. In this study, the stress concentration is due to geometrical wall thinning that would occur due to corrosion or erosion; it may be that other mechanisms such as fatigue may involve local dislocation enhancement or porosity, which act as local pinning points for Bloch wall movement [55]. These local pinning points are magnetic dipoles which may increase self-magnetization.

6. Conclusions

The magneto-mechanical memory (MMM) signal on the surfaces of L80 and 20 other structural steel specimens was recorded by AMR sensor arrays. The results show evidence of the residual magnetic leakage field (RMLF) signal due to applied load and the presence of notches as would be expected. A matched filter was applied to the results in order to extract the small perturbation on the magnetic signal. The main conclusions are:

- The stress history affects the MMM signal, but the effects are small in the steel samples tested.
- An irreversible change is seen in the initial elastic loading to a given load, while subsequent unloading and reloading at the same elastic stress level gives reversible changes.

- There is no evidence that plastic deformation builds up a cumulative magnetization; rather, it tends to erase the MMM signal.
- The perturbation of the magnetic signal due to notches without load is proportional to the applied magnetic field. Plastic deformation and residual stress generated around the notches after loading will increase the remanent flux leakage, but it remains small.

The results presented here showed no indication of the cumulative magnetoplastic effect that is required for the MMM as described by Dubov et al. to be capable of reliably detecting small areas of stress concentration. These observations suggest that the MMM effect is very small in the different grades of L80 pipeline steels and other structural steels that have been tested and it will not be a useful technique in practice in the field for these steel alloys.

Naturally, the absence of evidence for cumulative magnetization upon cyclic loading in our results does not constitute evidence of absence in general. Because of the obvious advantages of an NDE inspection method based on cumulative self-magnetization over other potential NDE methods available for assessment of remaining strength and service life, the NDE community cannot afford to give up on an opportunity like this. When a cumulative increase of RMLF is detected, special care will have to be taken to ascertain whether the effect is caused by increasing self-magnetization of the material or ordinary residual magnetic flux leakage caused by the nucleation and growth of otherwise undetectable microcracks. The influence of fatigue cracks (microcracks and marcocracks) on the MMM signal will be studied in further work. The 23 steels tested here are the start of an open data base and we encourage other researchers working in this field to contribute their results in the hope of establishing the specific conditions (alloying, temper, microstructure, hardness, etc.) under which the Metal Magnetic Memory method based on a cumulative magnetoplastic effect might be used reliably for quantitative materials characterization or, if that turns out to be not feasible, at least for pre-screening before more sophisticated inspection.

Acknowledgements

This work was supported by the UK Engineering and Physical Sciences Research Council (EPSRC), grant number EP/L022125/1, through the UK Research Centre in NDE (RCNDE).

References

[1] Liu X, Wang X. The research of oil and gas pipeline corrosion and protection technology. Advances in Petroleum Exploration and Development. 2014; 7: 102-5.

[2] Arora P, Singh PK, Bhasin V, Vaze KK, Pukazhendhi DM, Gandhi P, Raghava G. Fatigue crack growth behavior in pipes and elbows of carbon steel and stainless steel materials. Procedia Eng. 2013; 55: 703-9.

[3] Garland PJ. The importance of non-destructive testing and inspection of pipelines. Proceedings of 10th European Conference on Non-Destructive Testing 2010. 2010; 4: 2421-31 Curran Associates, Inc.

[4] Dubov, AA. A study of metal properties using the method of magnetic memory. Met. Sci. Heat Treat. 1997; 39: 401-5.

[5] Doubov, AA. Method of magnetic memory (MMM) of metal and inspection devices. Training handbook. Moscow: Energodiagnostika Co. Ltd; 2001.

[6] Dubov A. Energy diagnostics - is a physical basis of the metal magnetic memory method. In 19th World Conference on Non-Destructive Testing 2016.

[7] International Institute of Welding. Non-destructive testing - Metal magnetic memory - Part 1: Vocabulary (standard No. ISO 24497-1).

[8] International Institute of Welding. Non-destructive testing - Metal magnetic memory - Part 2: General requirements (standard No. ISO 24497-2).

[9] International Institute of Welding. Non-destructive testing - Metal magnetic memory - Part 3: Inspection of welded joints (standard No. ISO 24497-3).

[10] Dubov A, Kolokolnikov S. The metal magnetic memory method application for online monitoring of damage development in steel pipes and welded joints specimens. Weld. World.

2013; 57: 123-36.

[11] Dubov A, Kolokolnikov S. Assessment of the material state of oil and gas pipelines based on the metal magnetic memory method. Weld. World. 2012; 56: 11-19.

[12] Lin S, Wang W, Zhao C, Feng Z, Bi W, Jiang X. Application of metal magnetic memory method in long-distance oil and gas pipeline defects detection. Proceedings of the International Conference on Pipelines and Trenchless Technology. 2011; 973-80 American Society of Civil Engineers.

[13] Jiles DC. Theory of the magnetomechanical effect. J. Phys.D. App. Phys. 1995; 28: 1537-46.

[14] Atherton DL, Jiles DC. Effects of stress on magnetization. NDT Int. 1986; 19: 15-19.

[15] Kaleta J, Zebracki J. Application of the villari effect in a fatigue examination of nickel. Fatigue Fract. Engng Mater. Struct. 1996; 19: 1435-43.

[16] Willcox M, Dawnes G. A review of common nondestructive tests. The Tube & Pipe Journal. 2006; 17: 28-32.

[17] Nowakowski A, Paszylk P. Metal magnetic memory method used for analyzing high-pressure gas pipelines. AGH Drilling, Oil, Gas. 2015; 32: 395-404.

[18] Energodiagnostika Co. Ltd. Inspection devices for metal magnetic memory method, http://www.mmmsystem.com/Categories/Devices.html.

[19] Roskosz M, Gawrilenko P. Analysis of changes in residual magnetic field in loaded notched samples. NDT&E Int. 2008; 41:570-6.

[20] Shi C, Dong S, Xu B, He P. Stress concentration degree affects spontaneous magnetic signals of ferromagnetic steel under dynamic tension load. NDT&E Int. 2010; 43: 8-12.

[21] Roskosz M, Bieniek M. Evaluation of residual stress in ferromagnetic steels based on residual magnetic field measurements. NDT&E Int. 2012; 45: 55-62.

[22] Wilson JW, Tian G, Barrans S. Residual magnetic field sensing for stress measurement. Sensor Actuat. A Phys. 2007; 135: 381-7.

[23] Dong L, Xu B, Dong S, Song L, Chen Q, Wang D. Stress dependence of the spontaneous stray field signals of ferromagnetic steel. NDT&E Int. 2009; 42: 323-7.

[24] Leng J, Liu Y, Zhou G, Gao Y. Metal magnetic memory signal response to plastic deformation

of low carbon steel. NDT&E Int. 2013; 55: 42-6.

[25] Guo P, Chen X, Guan W, Cheng H, Jang H. Effect of tensile stress on the variation of magnetic field of low-alloy steel. J. Magn. Magn. Mater. 2011; 323: 2474-7.

[26] Li X, Ding H, Bai S. Research on the stress-magnetism effect of ferromagnetic materials based on three-dimensional magnetic flux leakage testing. NDT&E Int. 2014; 62: 50-4.

[27] Dong L, Xu B, Dong S, Chen Q, Dan W. Monitoring fatigue crack propagation of ferromagnetic materials with spontaneous abnormal magnetic signals. Int. J. Fatigue. 2008; 30: 1599-1605.

[28] Li C, Dong L, Wang H, Li G, Xu B. Metal magnetic memory technique used to predict the fatigue crack propagation behavior of 0.45%C steel. J. Magn. Magn. Mater. 2016; 405: 150-7.

[29] Huang H, Koamg S, Liu R, Liu Z. Investigation of magnetic memory signals induced by dynamic bending load in fatigue crack propagation process of structural steel. J. Nondestruct. Eval. 2014; 33: 407-12.

[30] Gorkunov ES. Different remanence states and their resistance to external effects. Discussing the so-called magnetic memory method. Insight - Non-Destructive Testing and Condition Monitoring. 2015; **57**: 709-17.

[31] Augustyniak M, Usarek Z. Discussion of derivability of local residual stress level from magnetic stray field measurement. J. Nondestruct. Eval. 2015; 34: 1-9.

[32] Usarek Z, Augustyniak B, Augustyniak M, Chmielewski M. Influence of plastic deformation on stray magnetic field distribution of soft magnetic steel sample. IEEE Trans. Magn. 2014; 50: 1-4.

[33] Leng J, Xu M, Zhou G, Wu Z. Effect of initial remanent states on the variation of magnetic memory signals. NDT&E Int. 2012; 52: 23-7.

[34] Huang H, Yao J, Li Z, Liu Z. Residual magnetic field variation induced by applied magnetic field and cyclic tensile stress. NDT&E Int. 2014; 63: 38-42.

[35] Hu B, Li L, Chen X, Zhong L. Study on the influencing factors of magnetic memory method. Int. J. Appl. Electrom. 2010; 33: 1351-7.

[36]Craik DJ, Wood MJ. Magnetization changes induced by stress in a constant applied field. J. Phys. D Appl. Phys. 1970; 3: 1009-16.

[37] Arkulis MB, Baryshnikov MP, Misheneva NI, Savchenko YI. On problems of applicability of the

metal magnetic-memory method in testing the stressed-deformed state of metallic constructions. Russ. J. Nondestruct. Test. 2009; 45: 526-8.

[38] Wu D, Xu M, Li J. Study on physical mechanism of metal magnetic memory technique. Applied Mechanics and Materials. 2010; 34-35: 841-4.

[39] Continental Alloys & Services. Alloy Steel, http://www.contalloy.com/materials/alloy-steel.

[40] SteelNumber: European Steel and Alloy Grades, http://www.steelnumber.com/index.php.

[41] West Yorkshire Steel. Steel Specifications, https://www.westyorkssteel.com/steel-specifications/.

[42] Otai Special Steel. http://www.astmsteel.com/.

[43] Woolman J, Mottram RA. The mechanical and physical properties of the British standard En steels (BS 970-1955): En 1 to En 20. Elsevier; 1964.

[44] Woolman J, Mottram RA. The mechanical and physical properties of the British standard En steels (BS 970-1955): En 21 to En 39. Elsevier; 1964.

[45] Woolman J, Mottram RA. The mechanical and physical properties of the British standard En steels (BS 970-1955): En 40 to En 363. Elsevier; 1964.

[46] Sensitec GmbH. AMR magnetic field sensors, http://www.sensitec.com/english/products/magnetic-field/aff755.html

[47] Shi Y, Zhang C, Li R, Cai M, Jia G. Theory and application of magnetic flux leakage pipeline detection. Sensors. 2015; 15: 31036-55.

[48] Chan PH, Tshai KY, Johnson M, Li S. The flexural properties of composite repaired pipeline: Numerical simulation and experimental validation. Compos. Struct. 2015; 133: 312-21.

[49] Jiang WC, Woo W, Wan Y, Luo Y, Xie XF, Tu ST. Evaluation of through-thickness residual stresses by neutron diffraction and finite-element method in thick weld plates. J. Press. Vess-T. ASME. 2017; 139: 031401.

[50] Jiles DC, Atherton DL. Theory of ferromagnetic hysteresis. J. Magn. Magn. Mater. 1986; 61: 48-60.

[51] Bozorth RM. Ferromagnetism. Hoboken: Wiley-IEEE Press; 1993.

[52] Dubov AA. Comprehensive diagnostics of the bends of boiler and steam-line tubes. Therm. Eng. 2007; 54: 712-5.

[53] Dubov AA. Experience with technical diagnostics of generator shroud rings at thermal plants. Therm. Eng. 2009; 56: 120-3.

[54]Dubov AA. Diagnostics of steam turbine disks using the metal magnetic memory method. Therm. Eng. 2010; 57: 16-21.

[55] Kobayashi S, Takahashi S, Kamada Y, Kikuchi, H, Ara, K. Magnetic minor hysteresis loops of compressively deformed transition-metal single crystals. J. Appl. Phys. 2006; 99: 08H908.

Appendix

The purpose of this appendix is to show the detailed chemical composition and mechanical properties of the steels used in the tests. The raw magnetic measurement data shown in Table 2 will be included in the electronic appendix upon publication.

TABLE I. Chemical composition of steels used in this paper (wt.%) [39-45].

	C	Mn	Mo	Cr	Ni	Cu	P	S	Si	V	other
4140-L80	0.38~0.43	0.75~1.0	0.15~0.25	0.8~1.1	≤0.25	≤0.25	≤0.025	≤0.025	≤0.35	≤0.3	Al<0.04
9CR-L80	≤0.15	0.3~0.6	0.9~1.1	8~10	≤0.5	≤0.25	≤0.02	≤0.01	≤1	-	-
13CR-L80	0.15~0.22	0.25~1	-	12~14	≤0.5	≤0.25	≤0.02	≤0.01	≤1	-	-
1.0570	≤0.20	1~1.6	≤0.08	≤0.3	≤0.3	-	≤0.035	≤0.035	≤0.55	0.02~0.15	-
1.2083	0.36~0.42	≤1.00	-	12.5~14.5	-	-	≤0.03	≤0.03	≤1.00	-	-
1.2312	0.35~0.45	1.4~1.6	0.15~0.25	1.8~2	-	-	≤0.03	0.05~0.1	0.3~0.5	-	-
1.2343	0.36~0.42	0.3~0.5	1.1~1.4	4.8~5.8	-	-	≤0.03	≤0.03	0.9~1.2	0.25~0.5	-
1.2363	0.95~1.05	0.4~0.8	0.9~1.2	4.8~5.5	-	-	≤0.03	≤0.03	0.1~0.4	0.15~0.35	-
1.2379/D2	1.45~1.6	0.2~0.6	0.7~1	11~13	-	-	≤0.03	≤0.03	-	0.7~1	-
1.2436	2~2.3	0.3~0.6	-	11~13	-	-	≤0.03	≤0.03	0.1~0.4	-	W 0.6~0.8
1.2510/O1	0.9~1.05	1~1.2	-	0.5~0.7	≤0.3	-	≤0.035	≤0.035	0.15~0.35	0.05~0.15	W 0.5~0.7
1.2767	0.4~0.5	0.2~0.5	0.15~0.35	1.2~1.5	3.8~4.3	-	≤0.03	≤0.03	0.1~0.4	-	-
1.7131	0.14~0.19	1~1.3	-	0.8~1.1	-	-	≤0.025	≤0.035	≤0.4	-	-
708M40	0.36~0.44	0.7~1	0.15~0.25	0.9~1.2	-	-	≤0.035	≤0.04	0.1~0.35	-	-
EN9	0.5~0.6	0.5~0.8	-	-	-	-	≤0.06	≤0.06	0.05~0.35	-	-
EN32	0.1~0.18	0.6~1	-	-	-	-	≤0.05	≤0.05	0.05~0.35	-	-
EN42	0.7~0.8	0.55~0.75	-	-	-	-	≤0.05	≤0.05	0.1~0.4	-	-
EN43	0.45~0.6	0.6~0.8	-	-	-	-	≤0.05	≤0.05	0.1~0.4	-	-
EN45	0.5~0.6	0.7~1	-	-	-	-	≤0.05	≤0.05	1.5~2	-	-
EN47	0.45~0.55	0.5~0.8	-	0.8~1.2	-	-	≤0.06	≤0.06	≤0.05	≥0.15	-
S275	≤0.25	≤1.6	-	-	-	-	≤0.04	≤0.05	≤0.05	-	-
S355J2+N	≤0.2	≤1.6	-	-	-	-	≤0.025	≤0.025	≤0.55	-	-
X65	0.04~0.16	1~1.6	-	-	-	-	≤0.035	≤0.035	≤0.55	-	-

TABLE II. Mechanical properties of steels used in this paper [39-45].

Steel	Yield strength (MPa)	Ultimate strength (MPa)
4140-L80	552	689
9CR-L80	552	655
13CR-L80	552	655
1.0570	345	470~630
1.2083	486	495
1.2312	620	859
1.2343	350~550	650~880
1.2363	450	750
1.2379/D2	550	850
1.2436	450	860
1.2510/O1	597	668
1.2767	645	880
1.7131	420	550
708M40	525	775~925
EN9	355	700
EN32	330	430
EN42	483	924
EN43	325	618
EN45	376	615
EN47	368	852
S275	275	410
S355J2+N	355	470~630
X65	448	530

Stress history affects the MMM signal; the effects are small in L80 materials tested.

Significant irreversible change always occurs only in the first loading cycle.

No evidence that plastic deformation builds up a cumulative magnetization.

The MMM effect is very small in the L80 alloy and structural steel samples tested.